Supporting information for

Construction of an aptamer-conjuncted molecular artificial enzyme with enhanced activity and selectivity

Yanjing Ke,[‡,a,b] *Xindi Li*,[‡,a] *Wenhui Shi*,[b] Yuze Han,[a] *Xin Peng* [a,d] and *Mengfan Wang*[*,a,c,d]

[a.] School of Life Sciences, Faculty of Medicine, Tianjin University, Tianjin 300072, P. R. China.

[b.] School of Chemical Engineering and Technology, State Key Laboratory of Chemical Engineering, Tianjin University, Tianjin 300350, P. R. China.

[c.] State Key Laboratory of Synthetic Biology. Tianjin University, Tianjin 300072, P. R. China.

[d.] Tianjin Key Laboratory of Function and Application of Biological Macromolecular Structures, Tianjin 300072, China.

‡ These authors contributed equally to this work.

* Corresponding email: mwang@tju.edu.cn (M.W.)

1. Supporting experimental

1.1 Materials

Iron (III) chloride hexahydrate ($FeCl_3$▪$6H_2O$) was purchased from Kemiou (Tianjin, China). Hydrogen peroxide (H_2O_2, 30%) was purchased from Aladdin (Shanghai, China). N-Hydroxysulfosuccinimide (NHS) was purchased from Shanghai yuanye Bio-Technology (Shanghai, China). 2,2':6',2''-Terpyridine, 2,2':6',2'-terpyridine-4'-carboxylic acid, methyl green (MeG), malachite green (MG) and 2-morpholinoethanesulfonic acid (MES) were purchased from Xiensi (Tianjin, China). 1-(3-dimethylaminopropyl)-3-ethylcarbodiimide (EDC) was purchased from Meryer (Shanghai, China). Crystal violet (CV) was purchased from Guangzhou chemical reagent factory (Guangzhou, China). Aptamers used in this study (**Table S1, Figure S6**) were purchased from GENEWIZ (Tianjin, China).

1.2 Fluorescence analysis

Equal volume of CV solution (1 μM) and aptamer solution (1 μM) were thoroughly mixed, and the fluorescence intensity at 571 nm was determined under the emission at 612 nm. The blank test was performed using PB buffer solution (0.1 M, pH 7.2) instead of the aptamer solution.

1.3 Molecular dynamics simulation

The molecular dynamics (MD) simulations were employed using Gromacs 2023.2 software package[1]. The Amber ff14SB force field[2] was utilized to pretreat aptamer molecules. The force field parameters and partial charges of Tpy(Fe) catalyst was built by Sobtop[3] and was refitted by restrained electrostatic potential (RESP) charge[4]. Each aptamer model is attached to Tpy(Fe) catalyst via a peptide bond, forming catalyst-aptamer molecules. The Apt-Tpy(Fe) structure was treated by Gaussian 09C[5] at TPSSh6[6]/def2SVP[7] method with geometry optimization and vibration analysis. The simulation system was then built by extending the Apt-Tpy(Fe) into a rectangular box with 0.8 nm margins. Each system was solvated with TIP3P water[8]. After undergoing 2000 steps of steepest descendent energy minimization and balanced simulation in 200

ps, stable Apt-Tpy(Fe) model was obtained. Subsequently, a CV molecule was placed into each Apt-Tpy(Fe) system and filled with TIP3P water. To equilibrate the system, an appropriate amount of Na+ ions were added. Then the energy minimization was performed again, followed by a 40 ns production simulation under the NPT ensemble. The distance between the geometric center of CV substrate and the Fe site of Apt-Tpy(Fe) was calculated every 1 ns. The temperature and pressure are controlled by velocity rescale thermostat[9] and stochastics cell rescale barostat[10]. The conformation was analyzed using Visual Molecular Dynamics (VMD) [11] and Discovery Studio Visualizer. The distances between CV molecule and Fe site were measured by using MDAnalysis Python library.

1.4 Molecular docking

The tertiary structure of the substrate was obtained from the ZINC database (https://zinc.docking.org/). The secondary structure of the aptamer was predicted using the RNA fold website (http://rna.tbi.univie.ac.at/cgi-bin/RNAWebSuite/RNAfold.cgi) and then submitted to the RNA Composer website for tertiary structure modeling (http://rnacomposer.ibch.poznan.pl/). Molecular docking was performed using AutoDock Vina[12] based on the structure of Apt-Tpy(Fe) after MD simulation, and the best docking results were analyzed and visualized by Pymol (www.pymol.org).

2. Supporting Figures

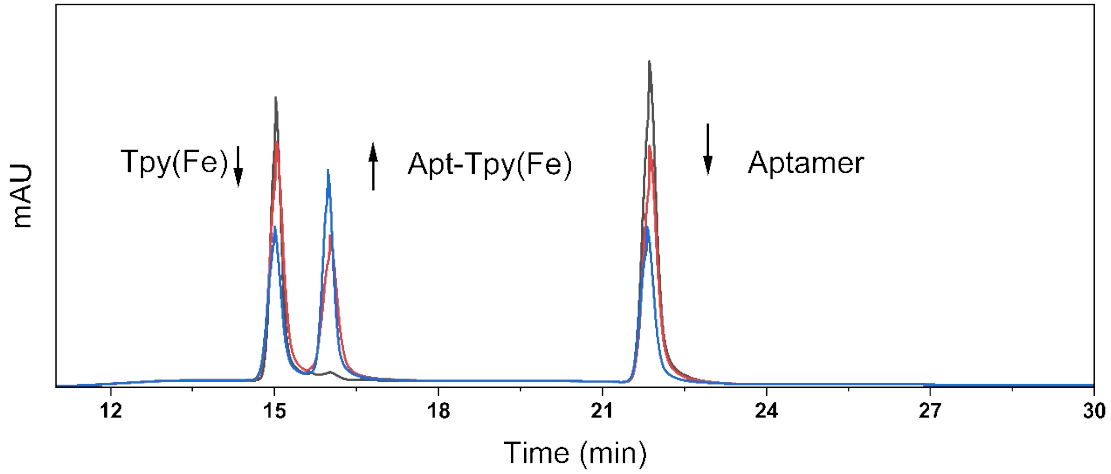

Figure S1. HPLC monitoring of the EDC/NHS reaction between amino-modified aptamer and Tpy(Fe).

The decreasing of Tpy(Fe) and aptamer together with the increasing of Apt-Tpy(Fe) indicated the formation of Apt-Tpy(Fe) conjugates.

HPLC condition: HPLC analyses were performed on a Shimadzu Prominence LC-20AT high-performance liquid chromatography system using a Grace Vydac 218TP C18 column (250 × 4.6 mm, 5 μm, 300 Å) under the detection wavelength of 260 nm. Mobile phase A consisted of 100 mM triethylammonium acetate buffer (pH 7.0), and mobile phase B was acetonitrile. Gradient elution program (0–5 min, hold at 5% B; 5–25 min, linear gradient to 35% B; 25–30 min, linear gradient to 60% B) was used with the flow rate of 1.0 mL/min.

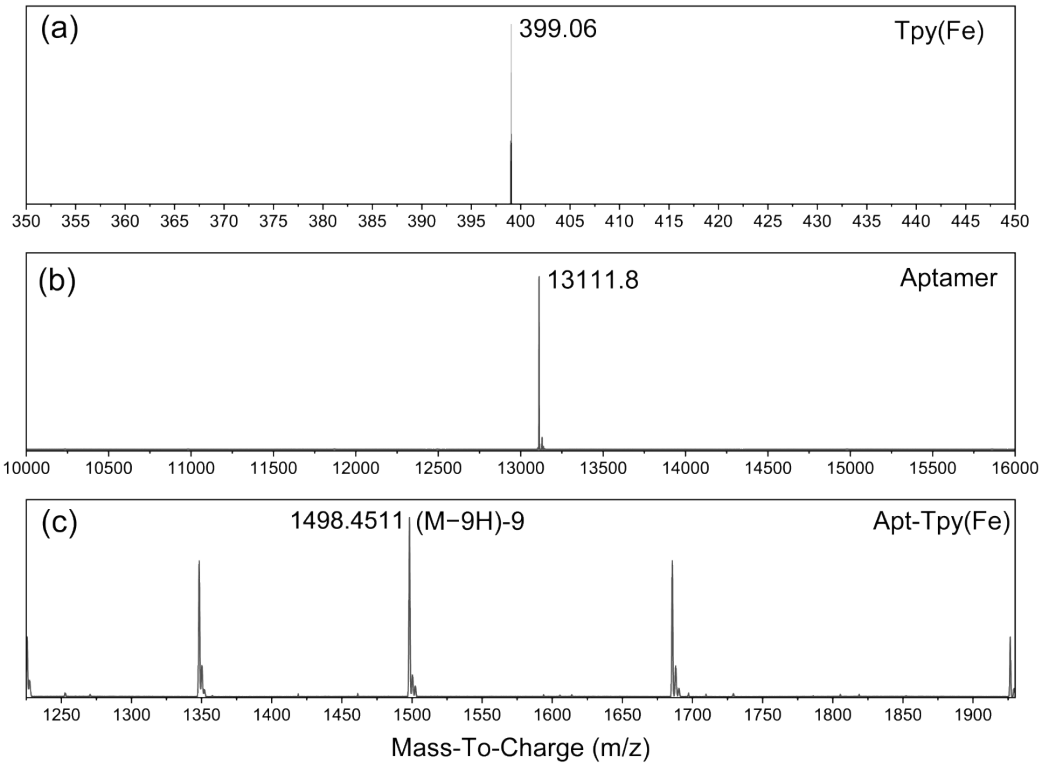

Figure S2. ESI-MS spectrum analysis of Tpy(Fe) (a), aptamer (b) and the conjunction product (c), which showing a multiply charged ion peak at m/z 1498.4511. For the 9^- charge state, this peak corresponds to a neutral molecular mass of approximately 13495.1 Da, supporting the successful formation of the Apt-Tpy(Fe) conjugate.

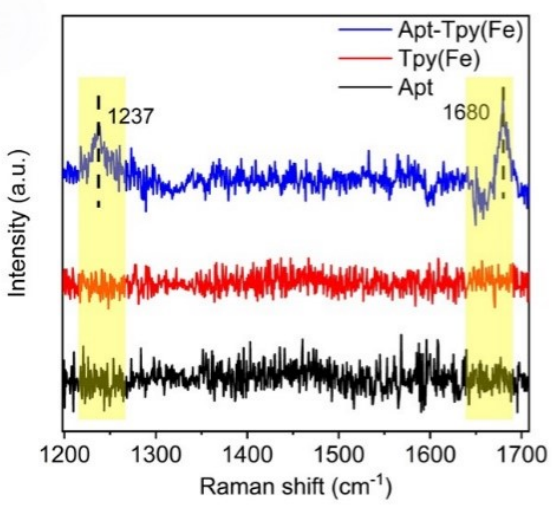

Figure S3. The Raman spectrum of CV aptamer (Apt), Typ(Fe) and Apt-Typ(Fe). The formation of –NH-CO- bond was verified by the characteristic Raman shifts at 1237 cm^{-1} and 1680 cm^{-1}

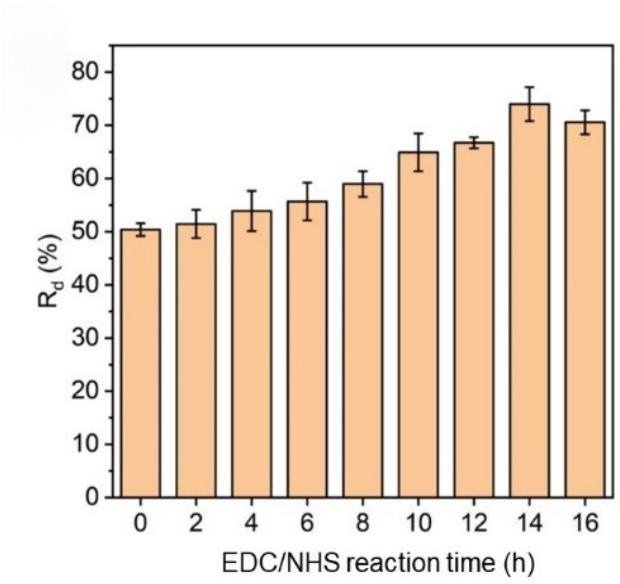

Figure S4. The effect of EDC/NHS reaction time on the degradation ability of Apt-Tpy(Fe) toward CV.

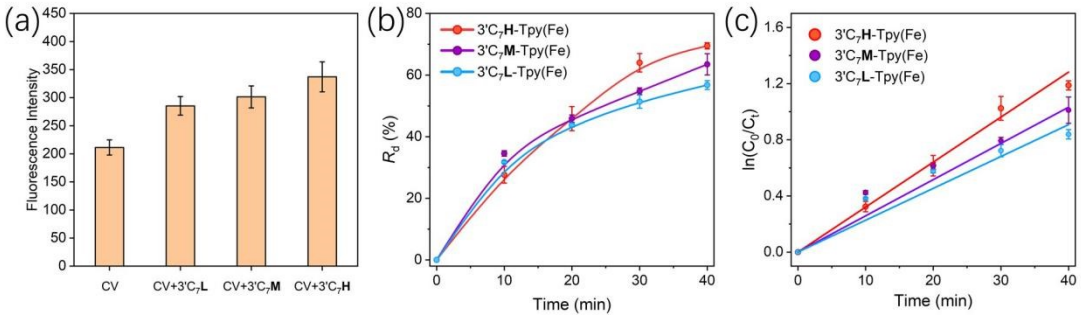

Figure S5. (a) Fluorescence analysis of CV that binds to aptamers with different affinities. Time-dependent degradation of CV (b) and reaction kinetics of CV degradation (c) catalyzed by 3'C_7**H**-Tpy(Fe), 3'C_7**M**-Tpy(Fe) and 3'C_7**L**-Tpy(Fe).

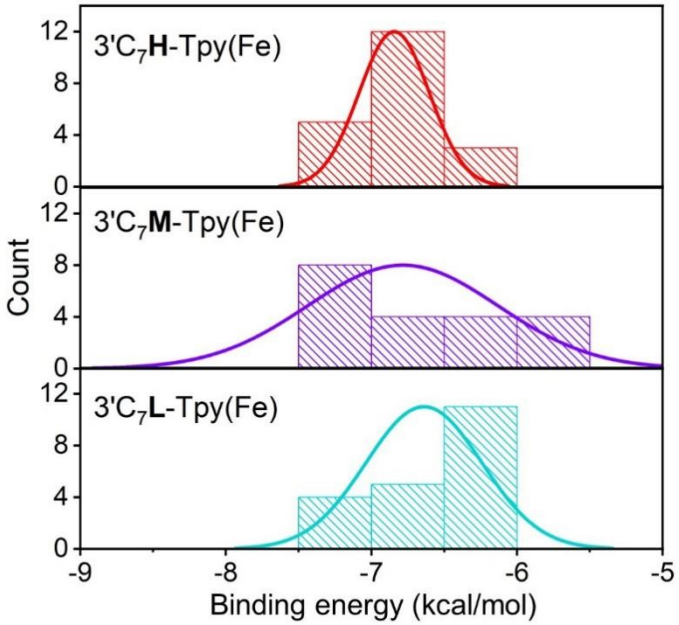

Figure S6. The frequency distribution of binding energy of 3'C_7**H**-Tpy(Fe), 3'C_7**M**-Tpy(Fe) and 3'C_7**L**-Tpy(Fe).

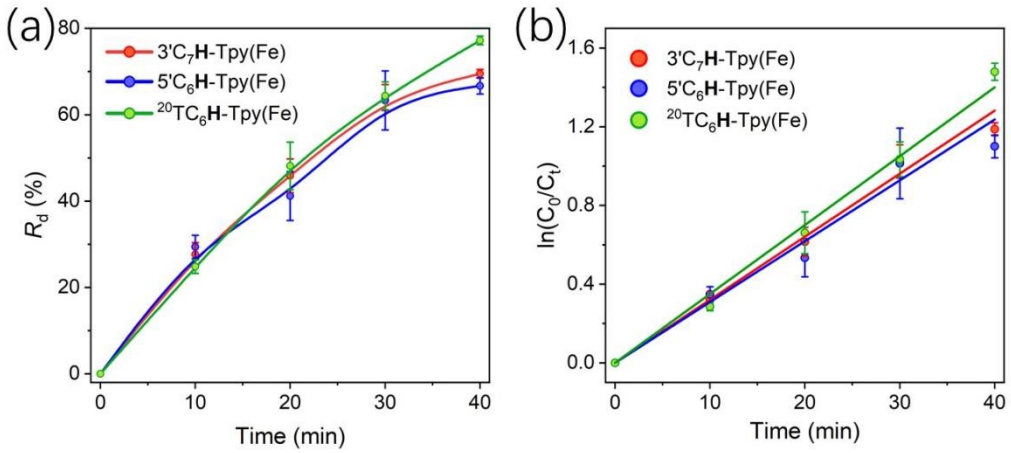

Figure S7. Time-dependent degradation of CV (a) and reaction kinetics of CV degradation (b) catalyzed by 3'C_7**H**-Tpy(Fe), 5'C_6**H**-Tpy(Fe) and $^{20}TC_6$**H**-Tpy(Fe).

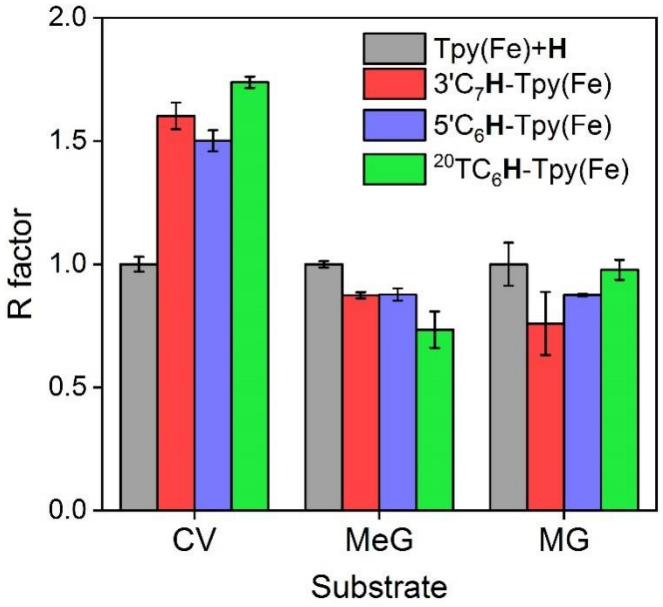

Figure S8. Catalytic selectivity of Apt-Tpy(Fe) for different substrates

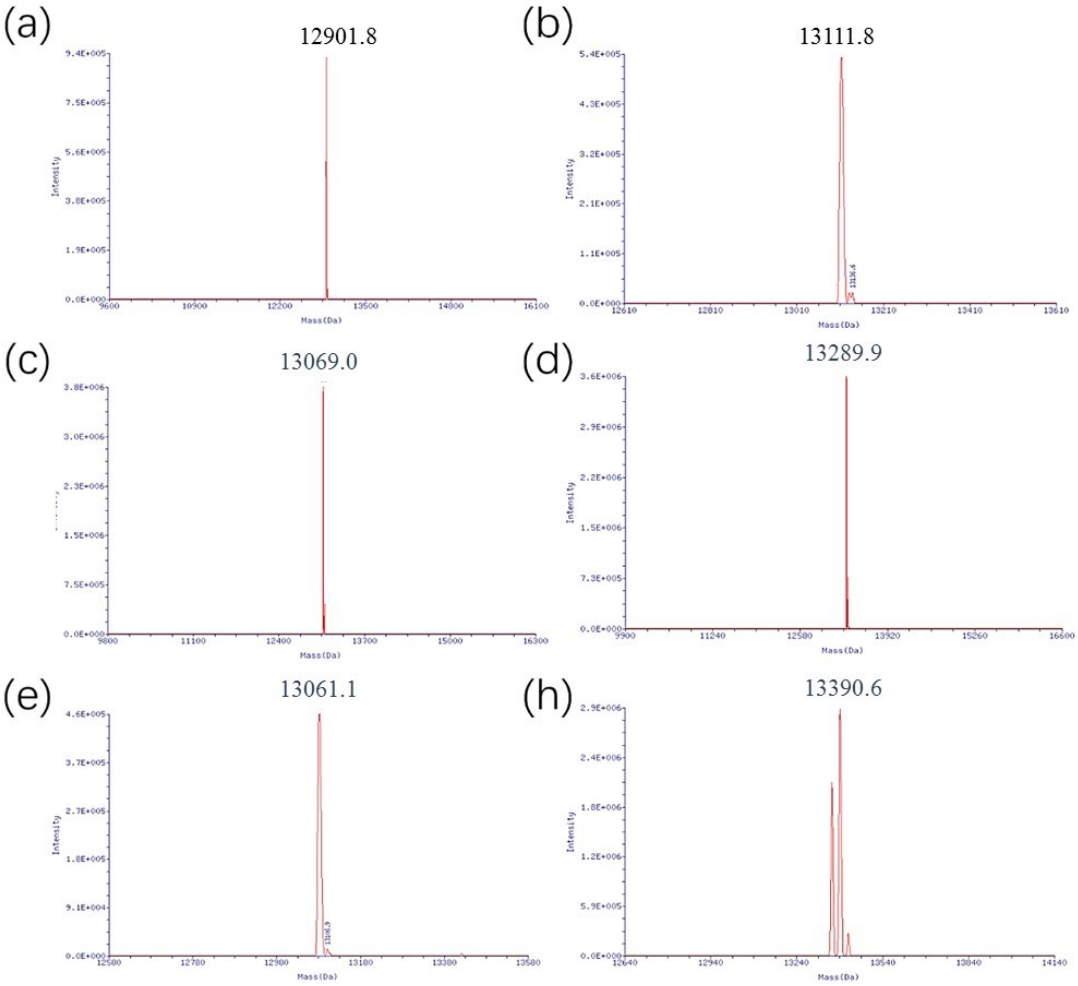

Figure S9. Mass spectrometry analysis of the aptamers used in this study: **H** (a), 3'C_7**H** (b), 3'C_7**M** (c), 3'C_7**L** (d), 5'C_6**H** (e) and ^{20}TC_6**H** (h).

3. Supporting Tables

Table S1. Sequences of aptamers used in this study

Aptamer	Sequence (5'→3')
H	AACGACCACCGGTGCGCCGTACAGGTAACTAGCGTCGTCGTT
M	AACGACGGGCTGGACGTCATCAACCTTCCACATGCAGTCGTT
L	AACGACACACACACTCTATATCATTAGCATGTACTCTGTCGTT
3'C_7**H**	AACGACCACCGGTGCGCCGTACAGGTAACTAGCGTCGTCGTT-**$(CH_2)_7$-NH_2**
3'C_7**M**	AACGACGGGCTGGACGTCATCAACCTTCCACATGCAGTCGTT-**$(CH_2)_7$-NH_2**
3'C_7**L**	AACGACACACACACTCTATATCATTAGCATGTACTCTGTCGTT **-$(CH_2)_7$-NH_2**
5'C_6**H**	**NH_2-$(CH_2)_6$-** AACGACCACCGGTGCGCCGTACAGGTAACTAGCGTCGTCGTT
^{20}TC_6**H**	AACGACCACCGGTGCGCCGT/**i$NH_2$$(CH)_6$dT**/ ACAGGTAACTAGCGTCGTCGTT

Table S2. The residues interact with CV molecule

Aptamer	Residues
3'C_7**H**-Tpy(Fe)	1A, 2A, 3C, 4G, 5A, 22C, 23A, 29C, 30T, 31A, 32G, 35T, 36C, 37G, 38T, 39C
5'C_6**H**-Tpy(Fe)	1A, 2A, 3C, 4G, 22C, 23A, 24G, 27A, 29C, 30T, 31A, 32G, 36C, 37G, 38T, 39C
^{20}TC_6**H**-Tpy(Fe)	2A, 3C, 4G, 21A, 22C, 23A, 31A, 32G, 33C, 36C

Table S3. R factor in the degradation of CV, MeG and MG

Substrate	Catalyst	R factor
CV	Tpy(Fe)+**H**	1.00
	3'C_7**H**-Tpy(Fe)	1.60
	5'C_6**H**-Tpy(Fe)	1.50
	^{20}TC_6**H**-Tpy(Fe)	1.74
MeG	Tpy(Fe)+**H**	1.00
	3'C_7**H**-Tpy(Fe)	0.87
	5'C_6**H**-Tpy(Fe)	0.88
	^{20}TC_6**H**-Tpy(Fe)	0.73
MG	Tpy(Fe)+**H**	1.00
	3'C_7**H**-Tpy(Fe)	0.76
	5'C_6**H**-Tpy(Fe)	0.87
	^{20}TC_6**H**-Tpy(Fe)	0.98

4. References

[1] Abraham, M. J.; Murtola, T.; Schulz, R.; Páll, S.; Smith, J. C.; Hess, B.; Lindahl, E. GROMACS: High performance molecular simulations through multi-level parallelism from laptops to supercomputers. *SoftwareX.* **2015,** *1-2*, 19-25.

[2] Maier, J. A.; Martinez, C.; Kasavajhala, K.; Wickstrom, L.; Hauser, K. E.; Simmerling, C. ff14SB: Improving the Accuracy of Protein Side Chain and Backbone Parameters from ff99SB. *J. Chem. Theory Comput.* **2015,** *11* (8), 3696-3713.

[3] Tian Lu, Sobtop, Version 1.0(dev3.1), http://sobereva.com/soft/Sobtop.

[4] Cornell, W. D.; Cieplak, P.; Bayly, C. I.; Kollman, P. A. Application of RESP charges to calculate conformational energies, hydrogen bond energies, and free energies of solvation. *J. Am. Chem. Soc.* **1993,** *115* (21), 9620-9631.

[5] Frisch, M. J.; Trucks, G. W.; Schlegel, H. B. *et al*. *Gaussian 09*, Revision C.01; Wallingford CT, **2016**.

[6] Staroverov, V. N.; Scuseria, G. E.; Tao, J.; Perdew, J. P. Comparative assessment of a new nonempirical density functional: Molecules and hydrogen-bonded complexes. *The Journal of Chemical Physics.* **2003,** *119* (23), 12129-12137.

[7] Weigend, F. Accurate Coulomb-fitting basis sets for H to Rn. *Phys. Chem. Chem. Phys.* **2006,** *8* (9), 1057-1065.

[8] Jorgensen, W. L.; Chandrasekhar, J.; Madura, J. D.; Impey, R. W.; Klein, M. L. Comparison of simple potential functions for simulating liquid water. *J. Chem. Phys.* **1983,** *79* (2), 926-935.

[9] Bussi, G.; Donadio, D.; Parrinello, M. Canonical sampling through velocity rescaling. *J. Chem. Phys.* **2007,** *126* (1), 014101.

[10] Bernetti, M.; Bussi, G. Pressure control using stochastic cell rescaling. *The Journal of Chemical Physics.* **2020,** *153* (11), 114107.

[11] Humphrey, W.; Dalke, A.; Schulten, K. VMD: Visual molecular dynamics. *J. Mol. Graphics.* **1996,** *14* (1), 33-38.

[12] Trott, O.; Olson, A. J. Software News and Update AutoDock Vina: Improving the Speed and Accuracy of Docking with a New Scoring Function, Efficient Optimization, and Multithreading. *Journal of Computational Chemistry.* **2010,** *31* (2), 455-461.